RESEARCH ARTICLE

Partially Coupled Inverse Model Design for Multivariable Disturbance Observer-Based Control Based on Generalized Relative Input Disturbance Gain

WU CAI[1], **PENG SHEN**[1], **YUTING SHANG**[1], **AND XINGHAN DU**[2]
[1]Department of Electrical Automation, Guangzhou Panyu Polytechnic, Guangzhou 511483, China
[2]College of Electrical Engineering and Automation, Jiangsu Normal University, Xuzhou 221116, China

Corresponding author: Wu Cai (buctcaiwu@163.com)

ABSTRACT In this paper, a novel inverse model is designed for multivariable disturbance observer-based (MDOB) control system. A new interaction measure, generalized relative input disturbance gain (GRIDG), is proposed to quantify the disturbance rejection capabilities of different inverse model structures. Consequently, an inverse model with partially coupled structure can be determined for better disturbance rejection performance. Besides, by defining a relative input disturbance gain array (RIDGA), the values of GRIDG under different input-output pairings and structures can be derived in an intuitive manner, which greatly facilitates the structure selection of the inverse model. And then, to overcome the difficulty of implementing the partially coupled inverse model, a V canonical structure is used without introducing model approximation. It also has the advantage of simple calculation and being easy to generalize to high-dimensional systems. Finally, simulation examples of several multivariable industrial processes are given to illustrate the design procedure and demonstrate the effectiveness of the proposed strategy.

INDEX TERMS Multivariable disturbance observer, partially coupled inverse model, generalized relative input disturbance gain, relative input disturbance gain array.

I. INTRODUCTION

Disturbances are widespread in industrial production and the suppression of disturbances has always been a primary problem. In process control, the systems commonly encountered are essentially multivariable systems with complex couplings, which are difficult to analyze and control since each system output is affected by the other loops. And therefore, disturbance rejection for multivariable systems is far from a simple problem. The directionality of multivariable system means that there are two possibilities for the effect of coupling on disturbance rejection — detrimental or beneficial. Given

The associate editor coordinating the review of this manuscript and approving it for publication was Engang Tian.

this, we may improve the disturbance rejection performance by making good use of couplings. For this purpose, two main issues need to be considered: (1) how to determine the effect of couplings on disturbance rejection, and (2) how to deal with the couplings.

There have been some discussions about the above problems under the framework of unit negative feedback control. Some interaction indices are proposed for coupling analysis from the perspective of disturbance rejection, e.g., Relative Disturbance Gain (RDG) [1], Disturbance Condition Number (DCN) [2], Closed Loop Disturbance Gain (CLDG) [3] and Relative Load Gain (RLG) [4]. With these indices, the influence of other loops' couplings can be quantified, and the multivariable controller utilizing couplings for disturbance

rejection can be designed. Two of the most widely studied controller design methods for this situation are the partially decentralized control [5], [6] (or sparse control [7]) and the partial decoupling control [8], [9]. The former aims to improve the disturbance rejection performance by specifying a particular controller structure, while the latter realizes different treatment of couplings by introducing a partial decoupler. Generally, these methods achieve better disturbance rejection performance than the typical decentralized and fully decoupled control.

Although in many cases the unit negative feedback control can eventually suppress disturbances by feeding back the error signals, the disturbance responses are relatively slow and the control system design is somewhat conservative. Thus, more effective disturbance rejection strategies should be researched and developed.

Disturbance observer-based (DOB) technique, first proposed by Ohnishi and his colleagues [10], [11], is a good attempt at this. DOB is a control strategy derived from practice and essentially a feedforward control. An estimation action is performed for disturbances based on the process input and output signals, and the estimates are used to counteract the effects of disturbances. Therefore, DOB can be applied to situations where disturbances are difficult or expensive to measure. Besides, the advantages of fast disturbance rejection speed, maintaining nominal performance in the absence of disturbance and easy implementation make DOB popular in various fields, such as motion control [12], process control [13], electrical engineering [14] and networked control system [15], etc.

At present, the research on DOB focuses on single-input-single-output (SISO) systems. In addition to the minimum phase (MP) plant [16], DOB design for plants with time delays [17], right-half-plane (RHP) zeros [18] and poles [19] are also discussed in detail. Improved DOB control structures in terms of time delay [17], non-minimum phase (NMP) dynamic [20] and noise [21] are putted forward. Analysis of the relationship between system robustness and bandwidth are carried out for NMP process [22] and system with real parameter uncertainty [23]. Besides, comprehensive optimization index [24] and data-driven algorithm [25] are utilized to further improve the DOB control system design.

Compared with the rich achievements of DOB in SISO system, the research on multivariable disturbance observer (MDOB) is still in the exploratory stage. The main difficulty lies in the design and implementation of the inverse model when couplings exist. Similar to the idea of decentralized control, a simple and intuitive way is to construct a diagonal inverse model based on the main channel transfer functions of the process, ignoring the couplings [26], [27]. It is a good solution for moderate interaction situations, but may cause performance deterioration when interactions are severe, since the neglected dynamics will burden the DOB for disturbance estimation and suppression. In view of this, another way for better performance is to obtain a relatively accurate and implementable inverse model by means of matrix manipulation and model approximation techniques [28], [29], [30]. The inverse model obtained in this way usually has a full element structure.

These are the two typical ways we currently design inverse models. Evidently, the diagonal and full element above are two of the most extreme structures for MDOB inverse models. Inspired by the partially decentralized controller in feedback control scheme, inverse model with other possible structures should also be explored for further performance improvements. Unfortunately, the authors did not find much research in this area. Last year, we did some tentative work. An interaction measure named relative input disturbance gain (RIDG) is proposed for evaluation of the disturbance rejection capabilities of MDOB under the two typical inverse model structures. A partially coupled inverse model with some rows identical to the full element inverse model and other rows identical to the diagonal inverse is then derived. Better disturbance responses have indeed achieved by the designed inverse model. Relevant results can be found in [31]. Nevertheless, we should realize that the above inverse model still does not have a general structure and the RIDG index is limited to evaluating the two extreme cases. More efforts should be made in this regard.

In this paper, coupling analysis is carried out for multivariable disturbance observer-based control system and a systematic inverse model design procedure is given. The main contributions of this paper are as follows:

1) Relationship between the disturbance rejection capability of MDOB and different inverse model structures is explored, and a new interaction measure, GRIDG, is proposed for performance evaluation and inverse model structure selection.

2) GRIDG is dependent on input-output pairing and the specific structure of the inverse model. By defining an interaction matrix RIDGA, the values of GRIDG under different input-output pairings and structures can be derived in an intuitive manner, which greatly facilitates the structure selection of the inverse model.

3) Based on the RIDGA-GRIDG results, an inverse model with partially coupled structure can be determined for better disturbance rejection performance. To our knowledge, this is the first inverse model with a general structure, which is different from any existing inverse model

4) A V canonical structure is used to implement the inverse model, without involving complicated calculations and model approximations.

This paper is organized as follows. In Section II, some preliminaries and analysis of MDOB inverse model are detailed. In Section III, the main points of this paper are elaborated, where the interaction measures, GRIDG and RIDGA, are proposed. Based on the evaluation results in Section III, design and implementation of the DOB filter are discussed in Section IV. Simulation studies are provided in Section V for two typical industrial processes. Finally, concluding remarks and future work are drawn in Section VI.
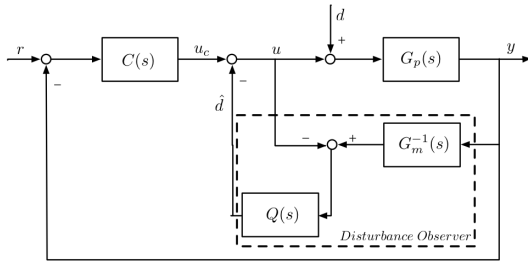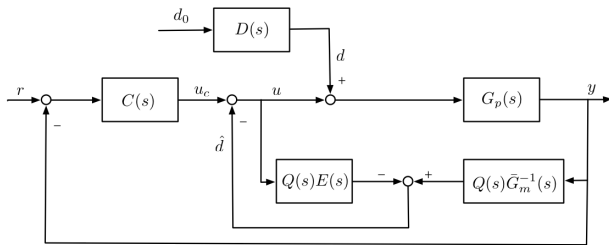
FIGURE 1. Basic MDOB control structure.

FIGURE 2. Improved MDOB structure in terms of time delays.

II. CONTROL STRUCTURE AND INVERSE MODEL ANALYSIS

A. MULTIVARIABLE DISTURBANCE OBSERVER-BASED (MDOB) CONTROL

The basic block diagram of MDOB control is shown in Fig. 1, where r, u_c, u, y, d and $\hat{d}$ are the vectors of reference inputs, controller outputs, manipulated variables, system outputs, external and estimated disturbances, respectively; $G_p(s)$ is the process transfer function matrix; $C(s)$ is the multivariable feedback controller; $G_m^{-1}(s)$ and $Q(s)$ are the inverse model and disturbance filter respectively, which are the components of the DOB structure and also the focus of our discussion.

In process control, the model $G_m(s)$ identified from real process usually contains multiple time delays, which bring difficulties to the design and analysis of the system. To reduce the influence of time delays, here, $G_m(s)$ is factorized as

$$G_m(s) = \bar{G}_m(s)E(s) \tag{1}$$

where $E(s)$ is a pure delay matrix and $\bar{G}_m(s)$ with smaller time delays is used for the inverse model design. Mathematically, $G_m(s)$, $\bar{G}_m(s)$ and $E(s)$ are expressed as $G_m(s) = [g_{ij}(s)]_{n \times n}$, $\bar{G}_m(s) = [\bar{g}_{ij}(s)]_{n \times n}$ and $E(s) = diag\{e^{-\tau_1 s}, e^{-\tau_2 s}, \dots, e^{-\tau_n s}\}$, respectively, where $\tau_j = min\{\tau_{1j}, \tau_{2j}, \cdots, \tau_{nj}\}$ is the minimum time delay of the jth column of $G_m(s)$. In this case, the control structure is modified to Fig. 2.

In Fig. 2, the delay matrix $E(s)$ is placed in the left input channel of DOB for synchronization and $Q(s)$ is multiplied together with the inverse model $\bar{G}_m^{-1}(s)$ for realizability. The closed-loop transfer function matrices from r and d_0 to y are derived as

$$\frac{y}{r} = G_p(I - QE + CG_p + Q\bar{G}_m^{-1}G_p)^{-1}C \tag{2}$$

$$\frac{y}{d_0} = G_p(I - QE + CG_p + Q\bar{G}_m^{-1}G_p)^{-1}(I - QE)D \tag{3}$$

where the disturbance is expressed as a product of a disturbance transfer function vector D and a normalized

disturbance d_0, i.e., $d = Dd_0$, and the Laplace variable s is omitted for simplicity hereafter. It is evident from (2) and (3) that setpoint tracking and disturbance rejection are related to both C and Q, which undoubtedly complicates our design. Given this, an independent design structure is adopted here, as shown in Fig. 3. And the input-output relationships become

$$\frac{y}{r} = G_p(I - QE + Q\bar{G}_m^{-1}G_p)^{-1}(I + CG_p)^{-1}C \tag{4}$$

$$\frac{y}{d_0} = G_p(I - QE + Q\bar{G}_m^{-1}G_p)^{-1}(I - QE)D \tag{5}$$

At this point, the disturbance response only depends on filter Q (see (5)). And therefore, a two-step design strategy can be used. Design Q first from the perspective of disturbance rejection. Substitute it into (4) and C is derived for setpoint tracking then.

In Fig. 3, it should be noted that the model mismatch is equivalently considered an internal disturbance d_{in} ($= (G_m^{-1}G_p - I)(u + d)$) here. Since modest uncertainties can be suppressed by DOB in a similar way to external disturbances, the discussion carried out following will focus on the external disturbance rejection problem in the nominal case.

B. INVERSE MODEL OF MDOB

As seen from (5), the inverse model $\bar{G}_m^{-1}$ has an impact on disturbance response through $(I - QE + Q\bar{G}_m^{-1}G_p)^{-1}$. Let $\bar{G}_x^{-1}$ denote an arbitrary stable inverse model. It is obvious that different $\bar{G}_x^{-1}$ results in different disturbance responses. In other words, the disturbance rejection capabilities provided by different $\bar{G}_x^{-1}$ are not the same. It is, however, very difficult to analyze the relationship between the inverse model and system output directly (see (5)). An intermediate variable, the estimated disturbance $\hat{d}$, is used to simplify the analysis here. This is feasible because $\hat{d}$ is related to both the inverse model and the disturbance estimate error $e_d = d - \hat{d}$, and the latter has an impact on system output.

According to the structural characteristics of $\bar{G}_x^{-1}$, the existing MDOB inverse model can be divided into two categories: (1) diagonal inverse model, whose elements obtained directly from the main channel elements of the process model; (2) full element inverse model derived from matrix manipulation, which usually involves model approximation. Their specific expressions are shown in (6) and (7), where g_{ii0} and $e^{-\tau_{ii}s}$ are the delay-free part and time delay of g_{ii}, respectively; the subscripts d and f represent the types of inverse model, i.e., diagonal or full element.

$$\bar{G}_d^{-1}(s) = [g_{ii0}^{-1}(s)]_{n \times n}, \quad E_d(s) = diag\{e^{-\tau_{ii}s}\}$$
$$i = 1, 2, \cdots, n \tag{6}$$

$$\bar{G}_f^{-1}(s) = \bar{G}_m^{-1}(s), \quad i, j = 1, 2, \cdots, n \tag{7}$$

In the case of $\bar{G}_f^{-1}$, the estimated disturbance in Fig. 3 is obtained as $\hat{d} = QEd$. Since Q and E are both diagonal matrices, from the perspective of coupling, we may think that $\bar{G}_f^{-1}$ realizes a complete decoupling from d to $\hat{d}$. As a result, the disturbance estimates avoid being affected by the inherent
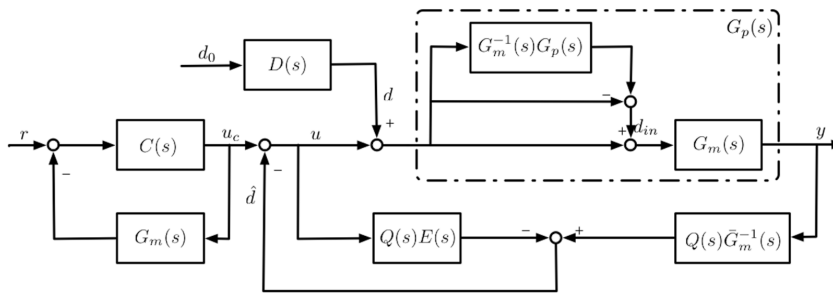
FIGURE 3. Modified MDOB control structure for independent design.

couplings of multivariable process and a relatively accurate $\hat{d}$ is obtained. On the contrary, $\bar{G}_d^{-1}$ is designed without any consideration or treatment of couplings. And the resulting $\hat{d}$ contains "full" coupling information. Obviously, the above two inverse models provide two extreme ways to deal with couplings, at least from the $\hat{d}$ standpoint. Therefore, an intuitive idea is: is there a more general inverse model be designed to selectively preserve the couplings in $\hat{d}$, so as to achieve better disturbance rejection performance? That is, the combined effect of the couplings in e_d and the process itself results in a smaller disturbance response y $(= G_m(e_d + u_c))$. And this is the starting point of our work for the partially coupled inverse model. In addition, note that the inverse model structure has a one-to-one correspondence with its coupling treatment for $\hat{d}$, the improved MDOB strategy will be developed around the structure design of the inverse model.

III. DISTURBANCE ANALYSIS INDICES
To find an inverse model structure that provides better disturbance rejection performance, an appropriate evaluation index should be discussed first. In this section, a generalized relative input disturbance gain (GRIDG) is proposed specifically for MDOB control scheme to quantify the disturbance rejection capabilities of inverse model with different structures. It is actually a generalized version of RIDG that we have defined earlier [31]. In addition, the matrix form of RIDG in terms of different loop pairings, relative input disturbance gain array (RIDGA), is putted forward for easy calculation of GRIDG.

A. RELATIVE INPUT DISTURBANCE GAIN (RIDG)
RIDG is defined as the ratio of disturbance response changes under two typical inverse models. From (5)-(7), we have

$$\left(\frac{\partial y}{\partial d_0}\right)_{(\bar{G}_d^{-1}, E_d)} = G_m(I - QE_d + Q\bar{G}_d^{-1}G_m)^{-1}(I - QE_d)D$$
(8)

$$\left(\frac{\partial y}{\partial d_0}\right)_{(\bar{G}_m^{-1}, E)} = G_m(I - QE)D$$
(9)

where the subscripts represent the cases of MDOB with diagonal and full element inverse models, respectively. Thus, RIDG is derived as

$$B = [\beta_i]_{n \times 1} = [G_m(I - QE_d + Q\bar{G}_d^{-1}G_m)^{-1}D] \odot (G_mD)$$
(10)

where $\odot$ denotes the element-by-element division and β_i is the ith element of RIDG. Terms $(I - QE_d)$ and $(I - QE)$ in (8) and (9) can be viewed as the parts of integral action $E(0) = E_d(0) = Q(0) = I$ and are omitted in the expression of RIDG. RIDG given in (10) contains the undetermined filter Q, and therefore the steady-state version is more commonly used, as shown in (11).

$$B(0) = [\beta_i^0]_{n \times 1} = (\bar{G}_d(0)D(0)) \odot (\bar{G}_m(0)D(0))$$
(11)

According to the definition of RIDG, the size of $|\beta_i^0|$ relative to 1 can be used to determine which of the two typical inverse models is recommended for loop i in terms of disturbance rejection. Thus, the RIDG-based structure selection rules are given as follows: (1) if $|\beta_i^0| > 1$, the couplings amplify the disturbance response and the full element inverse model $\bar{G}_f^{-1}$ is preferable; (2) if $|\beta_i^0| < 1$, the disturbance response is suppressed by the couplings and therefore the diagonal inverse model $\bar{G}_d^{-1}$ is recommended.

B. GENERALIZED RELATIVE INPUT DISTURBANCE GAIN (GRIDG)
RIDG above only give evaluation for the two typical MDOB inverse models. In this part, a more general index named GRIDG is proposed. Different from RIDG, GRIDG measures the disturbance rejection capability provided by a stable inverse model with arbitrary structure relative to the full element inverse model. The ith element of GRIDG is defined as

$$\beta_i' = \frac{\left(\frac{\partial y_i}{\partial d_0}\right)_{(\bar{G}_x^{-1}, E)}}{\left(\frac{\partial y_i}{\partial d_0}\right)_{(\bar{G}_m^{-1}, E)}}$$
(12)

and the vector forms are

$$B' = [\beta_i']_{n \times 1} = [G_m(I - QE + Q\bar{G}_x^{-1}G_m)^{-1}D] \odot (G_mD)$$
(13)

$$B'(0) = [\beta_i'^0]_{n \times 1} = (\bar{G}_x(0)D(0)) \odot (\bar{G}_m(0)D(0))$$
(14)

Compare (10) and (13), we found that RIDG is a special case of GRIDG when $\bar{G}_x^{-1}$ is taken as $\bar{G}_d^{-1}$ (or $\bar{G}_x = \bar{G}_d$). Similar to RIDG, the value of $|\beta_i'^0|$ can be used to determine the structure of $\bar{G}_x^{-1}$. To be specific, the structure giving smaller $|\beta_i'^0|$ value is better, as there is a quantitative relationship between $B'(0)$ and the integrated error (IE) under certain conditions.

Remark 1: If the DOB filter is $Q = diag\{Q_1, Q_2, \ldots, Q_n\}$ with $Q_i = 1/(\lambda_i s + 1)^{n_i}$, and the values of $\lambda_i n_i$ are the same for all of the n loops, we have

$$IE_x \odot IE_f = (\bar{G}_x(0)D(0)) \odot (\bar{G}_m(0)D(0)) = B'(0)$$

Remark 2: In this paper, the selection of the inverse model structure is mainly based on the steady-state indices, which may sometimes lead to inaccurate results. Our next work is to try to improve the accuracy of the evaluation results by introducing some available dynamic information.

C. RELATIVE INPUT DISTURBANCE GAIN ARRAY (RIDGA)

GRIDG is dependent on input-output pairing and the specific structure of $\bar{G}_x^{-1}$. However, it is not an easy work to find the optimal structure by traversing all possible inverse model structures under certain pairings. In view of this, a matrix form of RIDG, relative input disturbance gain array (RIDGA) derived for different pairings, is first defined here. Besides, to facilitate analysis, the structure selection of $\bar{G}_x$ is discussed instead that of $\bar{G}_x^{-1}$, as there is a correspondence between their structures.

With the definition of RIDG (shown in (10)), the ith element of RIDG for the case of $y_i - u_j$ pairing, denoted as β_{ij}, is obtained as

$$\beta_{ij} = \frac{\bar{g}_{ij}D_j}{\sum_{l=1}^{n} \bar{g}_{il}D_l} \quad (15)$$

at low frequencies ($E(j\omega) \approx I$, $Q(j\omega) \approx I$). And its matrix form, which is derived for different input-output pairings, is defined as

$$B_M \triangleq [\beta_{ij}]_{n\times n} = \bar{G}_m \otimes [ce(dg(D))] \otimes [re([dg(\bar{G}_m D)]^{-1})] \quad (16)$$

The second equation in (16) can be used to calculate RIDGA, where $dg(\cdot)$ is an operator that converts a vector into a diagonal matrix with the elements at diagonal positions; $ce(\cdot)$ and $re(\cdot)$ expand a diagonal matrix into a full element matrix whose ith column and row elements are all equal to the corresponding diagonal elements, respectively.

At this point, it is time to discuss the relationship between GRIDG, RIDGA and inverse model structures. First, to characterize the structure of $\bar{G}_x$, a structure selection matrix $\Gamma = [\kappa_{ij}]_{n\times n}$ is defined, where κ_{ij} is a bool variable. Two cases, $\kappa_{ij} = 0$ and $\kappa_{ij} = 1$, indicate the ijth entry of $\bar{G}_x$ is picked up or ignored, respectively. By this, $\bar{G}_x$ of a specific structure can be taken as

$$\bar{G}_{pc} = \bar{G}_m \otimes \Gamma \quad (17)$$

where $\otimes$ is the Hadamard product. The corresponding inverse model $\bar{G}_{pc}^{-1}$ obtained in this way is referred to as the partially coupled inverse model in this paper. And then, deduced from (13), the ith element of GRIDG for $\bar{G}_{pc}$ (or $\bar{G}_{pc}^{-1}$) is obtained as

$$\beta'_{i,pc} = \frac{\sum_{k=1}^{n} \bar{g}_{ik}\kappa_{ik}D_k}{\sum_{l=1}^{n} \bar{g}_{il}D_l} = \sum_{k=1}^{n} \left[\frac{\bar{g}_{ik}D_k}{\sum_{l=1}^{n} \bar{g}_{il}D_l} \right] = \sum_{k=1}^{n} \beta_{ik}\kappa_{ik} \quad (18)$$

at low frequencies. Simple calculations performed in (18) shows that $\beta'_{i,pc}$ is numerically equal to the ith row sum of matrix $B_M \otimes \Gamma$ ($= [\beta_{ij}\kappa_{ij}]_{n\times n}$). In this case, the GRIDG of an inverse model with any possible structure can be easily calculated by RIDGA. Some rules for $\bar{G}_{pc}$ structure selection are summarized as follows:

1) Calculate RIDGA by (16) and GRIDG of a specific structure can be derived directly (row sum).
2) The selected structure should has GRIDG elements closest to 0.
3) GRIDG elements $\beta'^0_{i,pc}$ greater than 1 or less than -1 should be avoided.

Remark 3: To simplify the design and ensure the non-singularity of the inverse model, all diagonal elements are picked up for $\bar{G}_{pc}$ in this work, i.e, $\kappa_{ii} = 1$, $i = 1, \cdots, n$.

To illustrate the above design procedure, a four-room Heating Ventilation and Air Conditioning (HVAC) system [32] is discussed here, as shown in (19), at the bottom of the next page.

The system is assumed to be disturbed by a unit step normalized disturbance $d_0 = 1/s$ with $D = [-1 \quad 0.5 \quad 0.6 \quad 0.8]^T$. Substituting $\bar{G}_m(0)$, $\bar{G}_d(0)$ and D into (11), the steady-state RIDG is calculated as $B(0) = [1.6897 \quad 2.3958 \quad 0.7321 \quad 0.8789]^T$. Similarly, based on (16), we have

$$B_M = \begin{bmatrix} 1.6897 & -0.3103 & -0.1448 & -0.2345 \\ -2.2396 & 2.3958 & 0.3437 & 0.5000 \\ -0.1435 & 0.0957 & 0.7321 & 0.3158 \\ -0.1322 & 0.0763 & 0.1770 & 0.8789 \end{bmatrix}$$

And as expected, the elements of $B(0)$ are equal to the diagonal elements of B_M.

With B_M, the structure giving smaller values of row sums is specified as

$$\Gamma = \begin{bmatrix} 1 & 1 & 1 & 1 \\ 1 & 1 & 0 & 0 \\ 1 & 0 & 1 & 0 \\ 1 & 0 & 0 & 1 \end{bmatrix}$$

and accordingly, the partially coupled model is determined as

$$\bar{G}_{pc} = \bar{G}_m \otimes \Gamma = \begin{bmatrix} \bar{g}_{11} & \bar{g}_{12} & \bar{g}_{13} & \bar{g}_{14} \\ \bar{g}_{21} & \bar{g}_{22} & 0 & 0 \\ \bar{g}_{31} & 0 & \bar{g}_{33} & 0 \\ \bar{g}_{41} & 0 & 0 & \bar{g}_{44} \end{bmatrix} \quad (20)$$

Here, to verify the relationship between GRIDG and RIDGA, $B'(0)$ derived from B_M and Γ is $[1 \quad 0.1562 \quad 0.5886 \quad 0.7467]^T$, which is consistent with that of $B'(0)$ calculated directly from (14). It is clear that the structure selection of $\bar{G}_{pc}$ can be easily carried out by the RIDGA-GRIDG method presented above.

IV. DESIGN OF THE INVERSE MODEL AND FILTER

The partially coupled inverse model is usually difficult to calculate and implement. In this paper, a V canonical structure is utilized to describe $\bar{G}_{pc}^{-1}$. It has the advantage of simple

calculation and being easy to generalize to high-dimensional systems.

A. PARTIALLY COUPLED INVERSE MODEL

Generally, the matrix inversion and model approximation techniques can be used to derive $\bar{G}_{pc}^{-1}$. These methods, however, involve complex calculation and the resulting error increases with the system size, which inevitably deteriorate the system performance. Fortunately, the V canonical structure is an effective solution for this problem. In Fig. 4, $Q\bar{G}_{pc}^{-1}$ is replaced equivalently by the structure in the dotted box, where the V canonical structure is implemented by matrix D_1 in the direct path and D_2 in the feedback path. One may note that a new filter Q' is used here instead of Q, which allows for more flexibility in designing matrices D_1 and D_2.

Based on Fig. 4, for disturbance rejection, it requires

$$QE = Q'D_1(I - D_2D_1)^{-1}G_m \quad (21)$$

Take the inverse of both sides of (21) and perform simple operations, we have

$$D_1^{-1} - D_2 = \bar{G}_m Q^{-1} Q' \quad (22)$$

Equation (22) can be used to determine matrices D_1 and D_2. To simplify the design and for the convenience of calculation, D_1 is selected as $D_1 = diag\{\delta_1, \delta_2, \ldots, \delta_n\}$ and D_2 is a matrix with zero elements at diagonal positions, i.e., $D_2 = [\rho_{ij}]_{n \times n}$, $\rho_{ii} = 0$. Filters Q and Q' are expressed as $Q = diag\{Q_1, Q_2, \ldots, Q_n\}$ and $Q' = diag\{Q_1', Q_2', \ldots, Q_n'\}$, respectively. Thus by (22), δ_i and ρ_{ij} can be derived as

$$\begin{cases} \delta_i = \dfrac{1}{\bar{g}_{ii}} \dfrac{Q_i}{Q_i'} \\ \rho_{ij} = -\bar{g}_{ij} \dfrac{Q_j'}{Q_j}, i \neq j \end{cases} \quad i,j = 1, 2, \cdots, n \quad (23)$$

where $\bar{g}_{ij}$ is the ijth elements of $\bar{G}_m$. Define $f_i = Q_i/Q_i'$, (23) simplifies to

$$\begin{cases} \delta_i = \dfrac{f_i}{\bar{g}_{ii}} \\ \rho_{ij} = -\dfrac{\bar{g}_{ij}}{f_j}, i \neq j \end{cases} \quad i,j = 1, 2, \cdots, n \quad (24)$$

In (24), f_i appears in both the numerator of δ_i and the denominator of ρ_{ij}. To guarantee the realizability of δ_i and ρ_{ij}, some requirements should be satisfied by f_i. Specifically, the time

delay, relative order and multiplicity of RHP zero of f_i should satisfy (25)-(27) respectively, where $\theta(x)$ represents the time delay of a transfer function x, $deg(x)$ and $\eta^k(x)$ denote the relative degree and multiplicity of the kth RHP zero of x, respectively.

$$\theta(\bar{g}_{jj}) \leq \theta(f_j) \leq \min_{i \neq j} \theta(\bar{g}_{ij}) \quad (25)$$

$$deg(\bar{g}_{jj}) \leq deg(f_j) \leq \min_{i \neq j} deg(\bar{g}_{ij}) \quad (26)$$

$$\eta^k(\bar{g}_{jj}) \leq \eta^k(f_j) \leq \min_{i \neq j} \eta^k(\bar{g}_{ij}) \quad (27)$$

Sometimes, not all the conditions given by (25)-(27) can be satisfied. In this case, a diagonal compensator $N = diag\{N_1, N_2, \ldots, N_n\}$ needs to be introduced. A general form of N_i is shown below.

$$N_i = \frac{1}{(\beta_i s + 1)^{r_i}} \prod_{j=1}^{k} \left(\frac{-s + z_j}{s + z_j^*} \right)^{t_{ij}} e^{-\tau_{N_i} s} \quad (28)$$

There are three parts of N_i: a low-pass term $1/(\beta_i s + 1)^{r_i}$ for properness, an all-pass term $\prod_{j=1}^{k}[(-s + z_j)/(s + z_j^*)]^{t_{ij}}$ for stability and an additional time delay $e^{-\tau_{N_i} s}$ for causality. In this way, the compensated process model becomes $G_m^N = NG_m$, and a new matrix $\bar{G}_m^N$ factorized from G_m^N ($= \bar{G}_m^N E'$) is used instead to design the inverse model. Accordingly, the elements of D_1 and D_2 are modified to

$$\begin{cases} \delta_i = \dfrac{f_i}{\bar{g}_{ii}^N} \\ \rho_{ij} = -\dfrac{\bar{g}_{ij}^N}{f_j}, i \neq j \end{cases} \quad i,j = 1, 2, \cdots, n \quad (29)$$

where $\bar{g}_{ij}^N$ is the ijth element of $\bar{G}_m^N$.

One should note that the pure time delay matrix E' here may not equal to the original E, and equation $\bar{G}_m^N = N\bar{G}_m$ does not hold. The reason is that the introduction of N may change the size of the common delay of each column. In view of this, a tactic for compensator introduction and inverse model design is given below.

The requirements shown in (25)-(27) can be used for pre-checking of compensator introduction by replacing $\bar{g}_{ij}$ with g_{ij} and omitting the inequalities about f_i. This is feasible because the separation of E from G_m will not affect the relative size of the ith column elements in terms of the time delay, relative order or multiplicity of the RHP zeros. Thus,

$$\begin{bmatrix} \dfrac{-0.098e^{-17s}}{122s+1} & \dfrac{-0.036e^{-27s}}{149s+1} & \dfrac{-0.014e^{-32s}}{158s+1} & \dfrac{-0.017e^{-30s}}{155s+1} \\ \dfrac{-0.043e^{-25s}}{147s+1} & \dfrac{-0.092e^{-16s}}{130s+1} & \dfrac{-0.011e^{-33s}}{156s+1} & \dfrac{-0.012e^{-34s}}{157s+1} \\ \dfrac{-0.012e^{-31s}}{153s+1} & \dfrac{-0.016e^{-34s}}{151s+1} & \dfrac{-0.102e^{-16s}}{118s+1} & \dfrac{-0.033e^{-26s}}{146s+1} \\ \dfrac{-0.013e^{-32s}}{156s+1} & \dfrac{-0.015e^{-31s}}{159s+1} & \dfrac{-0.029e^{-25s}}{144s+1} & \dfrac{-0.108e^{-18s}}{128s+1} \end{bmatrix} \quad (19)$$
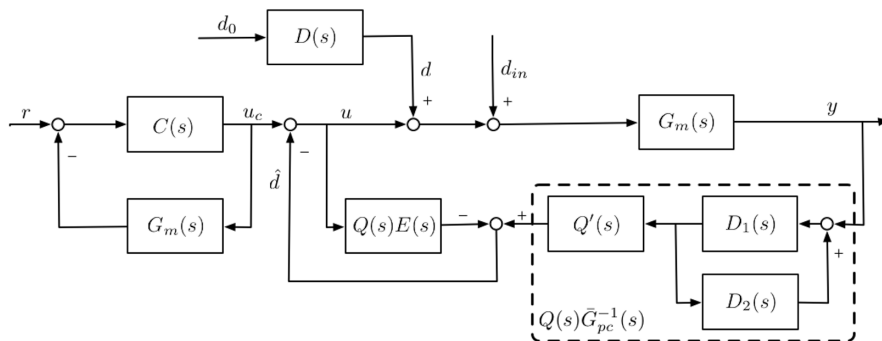
FIGURE 4. Modified MDOB based on the V canonical structure.

for a given process G_m, we may first check whether the constraints given by (25)-(27) are satisfied. If not, introduce the compensator N. Then, the factorization of time delay, design of the inverse model and filter are performed based on the compensated $\bar{G}_m^N$. In this way, some repetitive design procedures can be omitted.

From (29), N_i and f_i should be specified to obtain δ_i and ρ_{ij}. Let us focus on the design of N_i first. Based on the above derivation, N_i actually compensates all the ith row elements of G_m. Therefore, parameters of N_i, i.e., r_i, t_{ij} and τ_{N_i}, should be tuned to satisfy (25)-(27) for every $j(j = 1, 2, \cdots, n)$. Besides, additional dynamics should be introduced as little as possible for design complexity and performance reasons, namely, smaller values of r_i, t_{ij} and τ_{N_i} are preferable. Thus, the issue of determining the parameters of N_i can be formulated as a linear programming problem shown in (30), where x_i represents r_i, t_{ij} or τ_{N_i}, $i, j = 1, 2, \cdots, n$; $x = [x_1, x_2, \cdots, x_n]^T$ is the parameter vector to be solved; A and b are the coefficient matrix and vector, respectively. The modified MDOB structure with a compensator is depicted in Fig. 5.

$$min \sum_{i=1}^{n} x_i \quad s.t. \, Ax \geq b, x_i \geq 0 \quad (30)$$

As for f_i, a simple but not unique way is to take $f_i = \bar{g}_{ii}^N$. In this case, D_1 reduces to a unit matrix and the elements of D_2 are

$$\rho_{ij} = -\frac{\bar{g}_{ij}^N}{\bar{g}_{jj}^N}, i \neq j, \quad i, j = 1, 2, \cdots, n \quad (31)$$

Remark 4: The V canonical structure cannot be applied to the case where the determinant of $\bar{G}_{pc}$ contains RHP zeros because this would cause system stability problems. Nevertheless, this method can be applied to a special case where the RHP zero appears in the same row of $\bar{G}_{pc}$.

B. MDOB FILTER

After obtaining the inverse model, the design of the MDOB filters, Q and Q', are studied in this part. According to equations $f_i = Q_i/Q_i'$ and $f_i = \bar{g}_{ii}^N$, Q_i' can be derived as

$$Q_i' = \frac{Q_i}{f_i} = \frac{Q_i}{\bar{g}_{ii}^N} \quad (32)$$

That is, Q_i' is determined by a given Q_i. A simple and commonly used low-pass filter form is adopted for Q_i here, as shown in (33), where n_i is the order of Q_i and should satisfy the requirement given by (34) to ensure the properness of Q_i'; λ_i is the undetermined filter constant, which will be discussed in detail next.

$$Q_i = \frac{1}{(\lambda_i s + 1)^{n_i}} \quad (33)$$

$$n_i \geq deg(\bar{g}_{ii}^N) - r_i \quad (34)$$

Considering that robustness and performance have always been two major issues in control system design, and they usually have opposite requirements for the filter parameters, the selection of λ_i should give a good trade-off between these two aspects. Here, for robustness, the multiplicative input and output uncertainties, $G_P^I = G_m(I + \Delta_I)$ and $G_P^O = (I + \Delta_O)G_m$, are considered. The control system shown in Fig. 5 is transformed into the $M - \Delta$ structure for analysis, as illustrated in Fig 6. According to the small gain theorem, the necessary and sufficient condition for robust stability is

$$\bar{\sigma}(M_\varepsilon(j\omega)) < \frac{1}{\bar{\sigma}(\Delta_\varepsilon(j\omega))}, \quad \varepsilon = I, O, \forall \omega \quad (35)$$

where matrices M_I and M_O are derived as (36). The negative signs are omitted, as they would not affect the stability condition.

$$M_I = [I - QE + Q'D_1(I - D_2D_1)^{-1}NG_m]^{-1} \\ \cdot Q'D_1(I - D_2D_1)^{-1}NG_m$$
$$M_O = G_m[I - QE + Q'D_1(I - D_2D_1)^{-1}NG_m]^{-1} \\ \cdot Q'D_1(I - D_2D_1)^{-1}N \quad (36)$$

In terms of performance, the sensitivity function is known as a good measure and is obtained as (37), based on (5) and (21).

$$S = [I - QE + Q'D_1(I - D_2D_1)^{-1}NG_m]^{-1}(I - QE) \quad (37)$$

At last, the concrete value of λ_i can be determined by solving the optimization problem shown below.

$$min \quad \lambda_i$$
$$s.t. \begin{cases} \bar{\sigma}(M_\varepsilon(j\omega)) < \dfrac{1}{\bar{\sigma}(\Delta_\varepsilon(j\omega))}, \varepsilon = I, O \\ \bar{\sigma}(S(j\omega)) < \dfrac{1}{\bar{\sigma}(W_P(j\omega))} \end{cases} \forall \omega \quad (38)$$
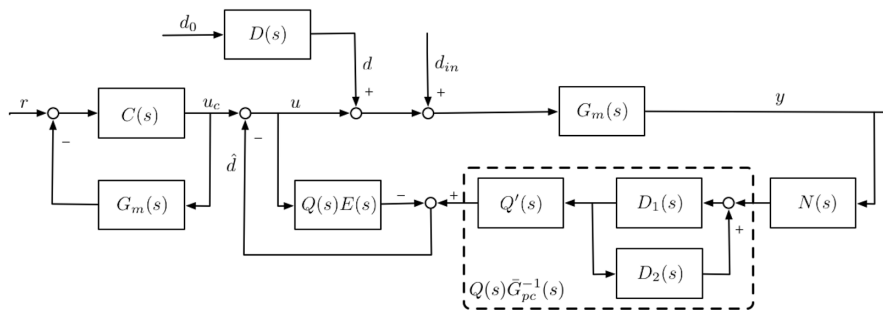
FIGURE 5. Modified MDOB structure with a compensator.

Continue with the previous HVAC example, we now consider the implementation of the partially coupled inverse model and compare the system disturbance rejection performance under different inverse model structures. The design procedures are given below.

1) Determine whether a compensator needs to be introduced. The elements of G_m (see (19)) are checked for the requirements given by (25)-(27). And it is found that there is no need to introduce a compensator, namely, $N = I$.

2) Determine the structure and concrete expression of $\bar{G}_{pc}$. G_m is written as

$$G_m = \bar{G}_m E$$

$$= \begin{bmatrix} g_{110} & g_{120}e^{-11s} & g_{130}e^{-16s} & g_{140}e^{-12s} \\ g_{210}e^{-8s} & g_{220} & g_{230}e^{-17s} & g_{240}e^{-16s} \\ g_{310}e^{-14s} & g_{320}e^{-18s} & g_{330} & g_{340}e^{-8s} \\ g_{410}e^{-15s} & g_{420}e^{-15s} & g_{430}e^{-9s} & g_{440} \end{bmatrix}$$

$$\cdot \begin{bmatrix} e^{-17s} & 0 & 0 & 0 \\ 0 & e^{-16s} & 0 & 0 \\ 0 & 0 & e^{-16s} & 0 \\ 0 & 0 & 0 & e^{-18s} \end{bmatrix} \quad (39)$$

and the $\bar{G}_{pc}$ with selected structure, which is shown in (20), can be derived accordingly.

3) The V canonical structure is used to implement $\bar{G}_{pc}^{-1}$. Let $f_i = \bar{g}_{ii}$, $i = 1, 2, \cdots, 4$, based on (29), matrices D_1 and D_2 are determined as

$$D_1 = I,$$

$$D_2 = \begin{bmatrix} 0 & \rho_{12} & \rho_{13} & \rho_{14} \\ \rho_{21} & 0 & 0 & 0 \\ \rho_{31} & 0 & 0 & 0 \\ \rho_{41} & 0 & 0 & 0 \end{bmatrix} \quad (40)$$

where the expressions of ρ_{ij}s are collected in Table 1.

4) Filter $Q = diag\{1/(\lambda_i s + 1)\}$, $i = 1, 2, \cdots, 4$, is used and Q' is obtained accordingly, as shown in (41). Filter parameters here are specified the same as reference [32] for simplicity, i.e., $\lambda_i = 45$, $i = 1, 2, \cdots, 4$.

$$Q' = diag\left\{ \frac{-(122s+1)}{0.098(\lambda_1 s+1)}, \frac{-(130s+1)}{0.092(\lambda_2 s+1)}, \right.$$
$$\left. \frac{-(118s+1)}{0.102(\lambda_3 s+1)}, \frac{-(128s+1)}{0.108(\lambda_4 s+1)} \right\} \quad (41)$$

TABLE 1. Elements of D_2 for HVAC.

$\rho_{12} = \dfrac{-0.036(130s+1)e^{-11s}}{0.092(149s+1)}$	$\rho_{13} = \dfrac{-0.014(118s+1)e^{-16s}}{0.102(158s+1)}$
$\rho_{14} = \dfrac{-0.017(128s+1)e^{-12s}}{0.108(155s+1)}$	$\rho_{21} = \dfrac{-0.043(122s+1)e^{-8s}}{0.098(147s+1)}$
$\rho_{31} = \dfrac{-0.012(122s+1)e^{-14s}}{0.098(153s+1)}$	$\rho_{41} = \dfrac{-0.013(122s+1)e^{-15s}}{0.098(156s+1)}$

TABLE 2. IE values and disturbance evaluation indices for HVAC.

G_m^{-1} Structure	IE_1	IE_2	IE_3	IE_4
Diagonal	6.060	-2.790	-3.735	-5.439
Full	3.612	-1.147	-5.137	-6.151
Partial	3.612	-0.144	-2.991	-4.635
$B'(0)$	1.0000	0.1563	0.5885	0.7467

Fig. 7 depicts the disturbance responses provided by the diagonal, full element and the proposed partially coupled inverse model structures. Evidently, $\bar{G}_{pc}^{-1}$ achieves better performance than the other two types. The IE and GRIDG values are collected in Table 2. And the quantitative relationship between them has been confirmed in this specific case.

V. SIMULATION RESULTS

In this section, two examples are performed to illustrate the design procedure and effectiveness of the proposed strategy. The output response is evaluated by two commonly used metrics: the integrated absolute error (IAE) and total variation (TV). And the robustness index γ [33] is used to quantify the system robustness. Their definitions are shown below.

$$IAE = \sum_{i=1}^{n} IAE_i, \quad IAE_i = \int_0^{\infty} |e_i(t)| dt$$

$$TV = \sum_{i=1}^{n} TV_i, \quad TV_i = \sum_{i=1}^{n} |u_i(k+1) - u_i(k)|$$

$$\gamma = \min_{\omega}(1/||M(j\omega)||), \quad \forall \omega \quad (42)$$

A. SIMULATION RESULTS OF VINANTE AND LUYBEN COLUMN

Consider the Vinante and Luyben (VL) column [34] (the time scale is in minutes):

$$G_m(s) = \begin{bmatrix} \dfrac{-2.2e^{-s}}{7s+1} & \dfrac{1.3e^{-0.3s}}{7s+1} \\ \dfrac{-2.8e^{-1.8s}}{9.5s+1} & \dfrac{4.3e^{-0.35s}}{9.2s+1} \end{bmatrix} \quad (43)$$
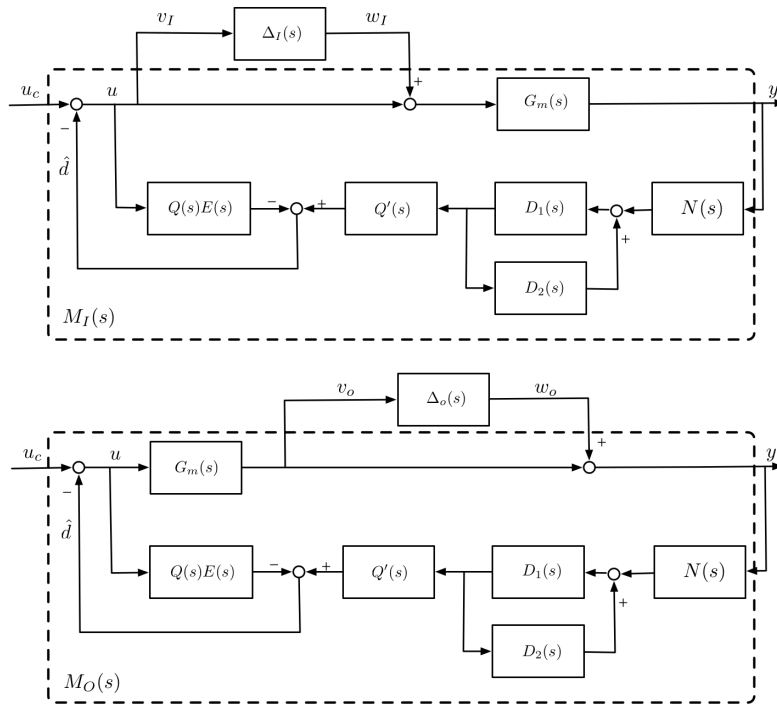
FIGURE 6. M-Delta structure of the modified MDOB.

Assume the disturbances occurring at the input are unit step signals with $D(s) = [1 \quad 0.3]^T$.

First of all, based on (16), RIDGA is calculated as

$$B_M = \begin{bmatrix} 1.2155 & -0.2155 \\ 1.8543 & -0.8543 \end{bmatrix}$$

and the structure $\Gamma = \{(1, 1), (0, 1)\}$ giving small values in GRIDG is selected. The requirements shown in (25)-(27) are checked and we find that g_{22} does not satisfy the time delay condition. Therefore, a compensator $N(s) = diag\{e^{-0.05s}, 1\}$ is introduced. Design of the inverse model will be carried out based on this compensated G_m^N.

Next, as stated, G_m^N is factorized as

$$G_m^N(s) = \bar{G}_m^N(s)E(s) = \begin{bmatrix} \dfrac{-2.2}{7s+1} & \dfrac{1.3}{7s+1} \\ \dfrac{-2.8e^{-0.75s}}{9.5s+1} & \dfrac{4.3}{9.2s+1} \end{bmatrix}$$
$$\cdot \begin{bmatrix} e^{-1.05s} & 0 \\ 0 & e^{-0.35s} \end{bmatrix} \quad (44)$$

and accordingly, $\bar{G}_{pc}^N$ for deriving the partially coupled inverse model is determined as

$$\bar{G}_{pc}^N(s) = \bar{G}_m^N(s) \otimes \Gamma = \begin{bmatrix} \dfrac{-2.2}{7s+1} & \dfrac{1.3}{7s+1} \\ 0 & \dfrac{4.3}{9.2s+1} \end{bmatrix} \quad (45)$$

For ease of calculation and implementation, let $f_i(s) = \bar{g}_{ii}^N(s)$, we have $D_1 = I$ and $\rho_{12}(s) = -\bar{g}_{12}^N(s)/\bar{g}_{22}^N(s) = -0.3(9.2s+1)/(7s+1)$ based on (31).
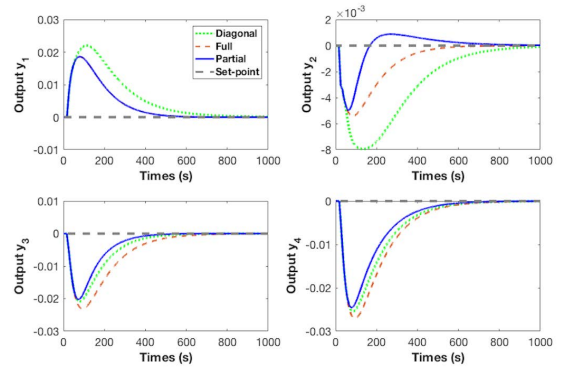

FIGURE 7. Disturbance responses under different inverse model structures.

Finally, filter $Q(s) = \{1/(\lambda_1 s+1), 1/(\lambda_2 s+1)\}$ is used and $Q'(s)$ is

$$Q'(s) = \begin{bmatrix} \dfrac{7s+1}{-2.2(\lambda_1 s+1)} & 0 \\ 0 & \dfrac{9.2s+1}{4.3(\lambda_2 s+1)} \end{bmatrix} \quad (46)$$

By solving the optimization problem shown in (38), parameters λ_i, $i = 1, 2$ are obtained as $\lambda_1 = 0.7$ and $\lambda_2 = 1$ under the following multiplicative uncertainties and performance matrices:

$$\Delta_I(s) = diag\left\{\dfrac{s+0.2}{1.2s+2}, \dfrac{s+0.3}{1.2s+2}\right\}$$

$$\Delta_O(s) = diag\left\{-\dfrac{s+0.3}{2s+1}, -\dfrac{s+0.1}{2s+1}\right\}$$
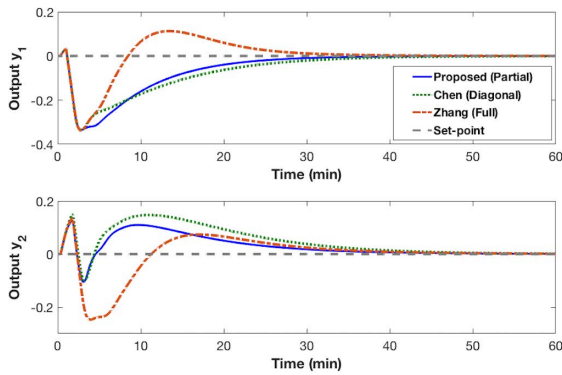
$$W_P(s) = \dfrac{10s+7}{25s+0.03} \cdot I$$
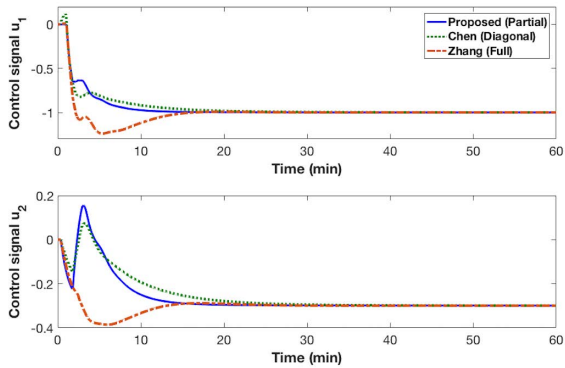
FIGURE 8. Disturbance responses for Example 1.

FIGURE 9. Control signals for Example 1.

TABLE 3. Performance and robustness indices for Example 1.

Methods	IAE_1	IAE_2	IAE	TV	γ_I	γ_O
Proposed	3.352	1.994	5.346	2.121	0.8936	0.8758
Chen	3.734	3.135	6.869	2.071	0.8733	0.7707
Zhang	2.753	2.662	5.415	2.422	0.5491	0.4152

Since the improved design of MDOB and disturbance rejection are the main objectives of this paper, the above method is compared with other two typical MDOB control strategies given by Chen *et al.* [26] and Zhang *et al.* [29]. The disturbance responses and control signals are plotted in Figs. 8 and 9, respectively. Note from Fig. 8 that satisfactory dynamics are provided by our scheme, especially for the second loop. And a slightly aggressive control signal for loop 2 is observed in Fig. 9. This is acceptable, since the smallest IAE values are obtained and the TV value of the proposed strategy is moderate (listed in Table 3). Apart from performance, the robust stability regions provided by these methods are depicted in Fig. 10. The minimums of these curves, which indicate the maximum magnitudes of the uncertainties that the system can tolerate, are also collected
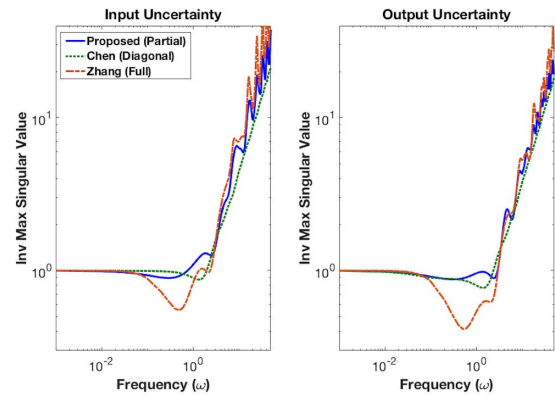

FIGURE 10. Robust stability bounds for Example 1.

in Table 3. Obviously, our control strategy gives the largest γ values for both input and output uncertainties, indicating the strongest stability robustness among them.

B. SIMULATION RESULTS OF OGUNNAIKE AND RAY PROCESS

Consider the Ogunnaike and Ray (OR) process given in reference [35], (47), as shown at the bottom of the page.

The input disturbance vector is assumed to be $D(s) = [0.5 \quad 0.2 \quad -2.5]^T$. Similar to the above design procedure for VL, the main design steps are as follows:

1) GRIDG-RIDGA based structure selection.
   By (16), RIDGA is obtained as

   $$B_M = \begin{bmatrix} 1.4983 & -0.5539 & 0.0556 \\ 5.1389 & -4.3704 & 0.2315 \\ 1.6876 & -0.8993 & 0.2117 \end{bmatrix}$$

   An appropriate structure giving smaller GRIDG values, i.e., $B'(0) = [0.9444 \quad 0.7685 \quad 0.2117]^T$, is determined as $\Gamma = \{(1, 1, 0), (1, 1, 0), (0, 0, 1)\}$.

2) Analysis and introduction of the compensator.
   By checking the conditions in (25)-(27), there is no need to introduce a compensator, that is, $N(s) = I$.

3) Inverse model implementation based on the V canonical structure.
   As before, the process model $G_m(s)$ is factorized as a time delay part $E(s)$ pre-multiplies a remaining matrix $\bar{G}_m(s)$. For OR column, it is

   $$G_m(s) = \bar{G}_m(s)E(s)$$
   $$= \begin{bmatrix} g_{110} & g_{120}e^{-0.5s} & g_{130} \\ g_{210}e^{-3.9s} & g_{220}e^{-3s} & g_{230}e^{-0.2s} \\ g_{310}e^{-6.6s} & g_{320}e^{-6.4s} & g_{330} \end{bmatrix}$$

$$G_m(s) = \begin{bmatrix} \dfrac{0.66e^{-2.6s}}{6.7s+1} & \dfrac{-0.61e^{-3.5s}}{8.64s+1} & \dfrac{-0.0049e^{-s}}{9.06s+1} \\[2mm] \dfrac{1.11e^{-6.5s}}{3.25s+1} & \dfrac{-2.36e^{-3s}}{5s+1} & \dfrac{-0.01e^{-1.2s}}{7.09s+1} \\[2mm] \dfrac{-34.68e^{-9.2s}}{8.15s+1} & \dfrac{46.2e^{-9.4s}}{10.9s+1} & \dfrac{0.87(11.61s+1)e^{-s}}{(3.89s+1)(18.8s+1)} \end{bmatrix} \tag{47}$$

$$\cdot \begin{bmatrix} e^{-2.6s} & 0 & 0 \\ 0 & e^{-3s} & 0 \\ 0 & 0 & e^{-s} \end{bmatrix}$$

The partially coupled model $\bar{G}_{pc}(s)$ is then determined by $\bar{G}_m(s)$ and Γ:

$$\bar{G}_{pc}(s) = \bar{G}_m(s) \otimes \Gamma$$

$$= \begin{bmatrix} g_{110} & g_{120}e^{-0.5s} & 0 \\ g_{210}e^{-3.9s} & g_{220}e^{-3s} & 0 \\ 0 & 0 & g_{330} \end{bmatrix} \quad (48)$$

To implement $\bar{G}_{pc}^{-1}(s)$, $f_i(s) = \bar{g}_{ii}(s)$ is selected as usual. And in this case, $D_1 = I$ and the elements of D_2 are calculated as

$$\rho_{12} = \frac{-\bar{g}_{12}}{\bar{g}_{22}} = \frac{-0.61(5s+1)e^{-0.5s}}{2.36(8.64s+1)}$$

$$\rho_{21} = \frac{-\bar{g}_{21}}{\bar{g}_{11}} = \frac{-1.11(6.7s+1)e^{-3.9s}}{0.66(3.25s+1)}$$

4) Filter parameters tuning.

At last, the diagonal weights for uncertainties and performance are specified as

$$\Delta_I(s) = diag\left\{ \frac{s+0.3}{s+25}, \frac{s+0.2}{s+25}, \frac{s+0.2}{s+25} \right\}$$

$$\Delta_O(s) = diag\left\{ -\frac{s+0.2}{8s+20}, -\frac{s+0.3}{8s+20}, -\frac{s+0.3}{8s+20} \right\}$$

$$W_P(s) = \frac{s/2.2 + 0.04}{25s + 0.15}I$$

respectively. $Q(s)$ has the same form as that of Example 1 and the parameters are tuned as $\lambda_1 = 3.1$, $\lambda_2 = 3.1$, $\lambda_3 = 3.2$ to satisfy the robust stability and performance requirements above.

Figs. 11 and 12 depict the system outputs and disturbance estimates under different inverse model structure cases. The corresponding IAE values are collected in Table 4. Obviously, form Fig. 11 and Table 4, the partially coupled inverse model we designed provides the best disturbance responses for all of the three loops in terms of the magnitudes, convergence speed and the error integral indices. Part of the reason is revealed in Fig.12 that almost the same disturbance estimates are produced by $\bar{G}_m^{-1}$ and $\bar{G}_{pc}^{-1}$ for loops 1 and 2, while a poor disturbance estimates is deliberately obtained by $\bar{G}_{pc}^{-1}$ for loop 3. The purpose of this action is to preserve the couplings that are beneficial to disturbance rejection. Besides, the simulation results verify that the RIDGA-GRIDG rule provides a simple and correct instruction for $\bar{G}_{pc}^{-1}$ structure selection.

The proposed strategy is compared with other multivariable control methods, i.e., the MDOB based decoupling control [29], enhanced decentralized control with DOB [13], sparse control [36] and centralized control [37]. The disturbance responses and control signals are plotted in Figs. 13 and 14, respectively. Table 5 lists the performance indices of these strategies. It is observed from Fig. 13 that the smallest overshoots of loops 1 and 2 and a moderate magnitude of loop
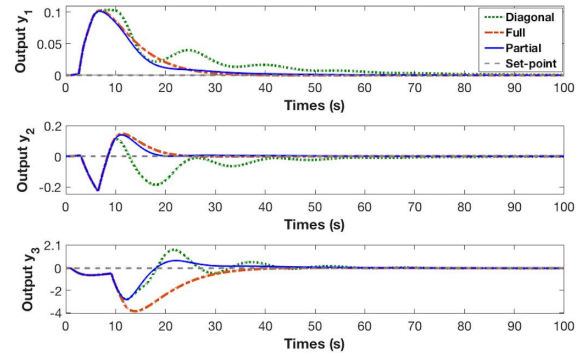

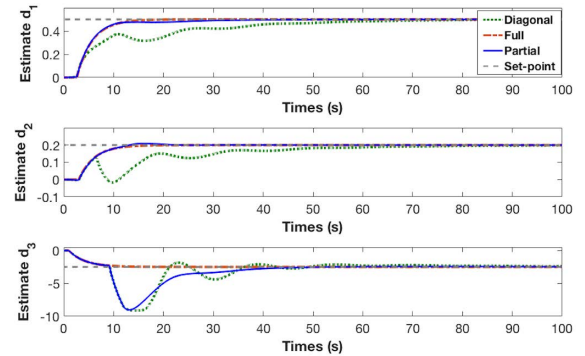**FIGURE 11.** Disturbance responses under different inverse model structures for Example 2.

FIGURE 12. Disturbance estimates under different inverse model structures for Example 2.

TABLE 4. Performance indices for Example 2 under different structures.

$\bar{G}_m^{-1}$ Structure	IAE_1	IAE_2	IAE_3	IAE
Diagonal	1.869	3.447	36.12	41.436
Full	1.194	1.720	52.79	55.704
Partial	1.138	1.592	28.28	31.010

TABLE 5. Performance indices for Example 2.

Methods	IAE_1	IAE_2	IAE_3	IAE	TV
Proposed	1.138	1.592	28.28	31.010	16.4125
Decoupling	1.172	1.761	50.17	53.103	3.2803
Sparse	2.550	3.697	15.34	21.587	53.8062
Decentralized	2.045	3.331	28.32	33.696	29.1544
Centralized	1.080	2.383	51.39	54.853	31.3236

3 are obtained by our method. Besides, relatively fast convergence speed also indicates the superior dynamic responses of the proposed strategy. It should be noticed that the sparse control gives much better dynamic performance and indices (shown in Table 5) than other methods for loop 3, but almost the worst disturbance responses for loops 1 and 2. That is, the sparse control cannot provide a good balance between control loops for this case. As for the control signals, Fig. 14 and Table 5 show that our strategy provides smoother inputs and smaller TV value than other methods except the decoupling control. It is, however, observed from Fig. 13 that the decoupling control approach suffer from a major disadvantage that the disturbance response presents poor dynamics and the IAE values are relatively large.

Fig. 15 depicts the robust stability regions of the above methods, and values of the robustness index γ are listed in
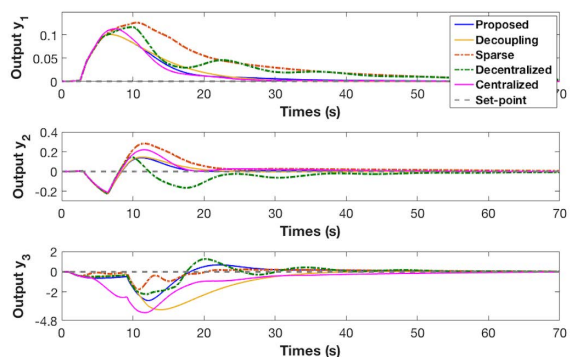
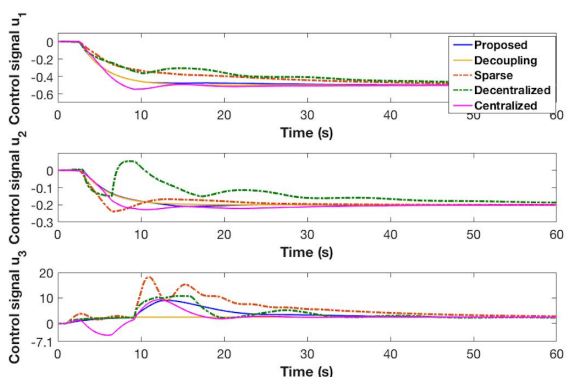**FIGURE 13.** Disturbance responses for Example 2.
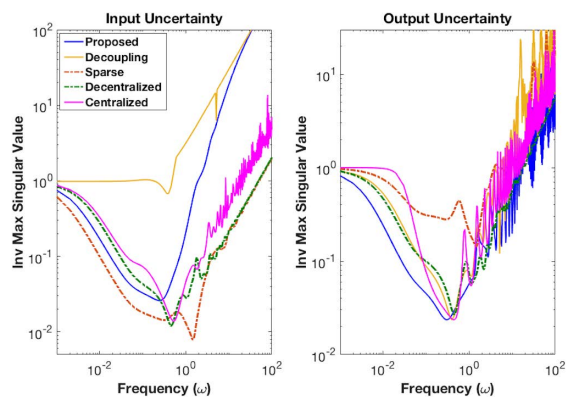

FIGURE 14. Control signals for Example 2.

FIGURE 15. Robust stability bounds for Example 2.

TABLE 6. Robustness indices for Example 2.

Methods	Input uncertainty (γ_I)	Output uncertainty (γ_O)
Proposed	0.0259	0.0235
Decoupling	0.6716	0.0234
Sparse	0.0078	0.1416
Decentralized	0.0118	0.0264
Centralized	0.0139	0.0235

Table 6. A relatively large γ_I, which is larger than that of other strategies except the decoupling control, is obtained by our approach. And for the output uncertainties, the proposed method also provides a moderate γ_O.

VI. CONCLUSION

In this paper, a modified inverse model design method is proposed for DOB strategy in cases of stable multivariable systems with time delays. Two main issues: the structure selection and implementation of the inverse model, are discussed in detail. Specifically, relationship between the disturbance rejection capability of MDOB and different inverse model structures is investigated. An interaction measure GRIDG is proposed for performance evaluation and inverse model structure selection. To facilitate the calculation of GRIDG, RIDGA is developed. As a result, GRIDG of different inverse model structures can be derived by calculating the corresponding row sums of RIDGA. Based on the RIDGA-GRIDG indices, rules for structure selection of the inverse model are provided. And a partially coupled inverse model can be determined for better disturbance rejection performance. This modified inverse model is implemented by a V canonical structure, which has the advantage of simple calculation and being easy to generalize to high-dimensional systems. Design of matrices D_1 and D_2 are discussed and a compensator will be introduced if necessary. Finally, filter parameters are tuned to satisfy both the performance and robustness requirements. The effectiveness and superiority of the proposed strategy is verified by simulation results.

The structure selection rules for MDOB inverse model proposed in this paper are mainly based on the steady-state forms of GRIDG and RIDGA. In future work, some available dynamic information will be introduced into the metrics to improve the accuracy of the evaluation results. Besides, other effective indices and inverse model design methods of MDOB systems are also our next step to study.

REFERENCES

[1] G. Stanley, M. Marino-Galarraga, and T. J. McAvoy, "Short cut operability analysis. 1. The relative disturbance gain," *Ind. Eng. Chem. Process Design Develop.*, vol. 24, no. 4, pp. 1181–1188, Oct. 1985.

[2] S. Skogestad and M. Morari, "Simple frequency-dependent tools for control system analysis, structure selection and design," *Ind. Eng. Chem. Res.*, vol. 26, no. 10, pp. 2029–2035, Oct. 1987.

[3] M. Hovd and S. Skogestad, "Effect of disturbance directions on closed-loop performance," *Automatica*, vol. 268, no. 5, pp. 989–996, Sep. 1992.

[4] H.-P. Huang, F.-Y. Lin, and J.-C. Jeng, "Control structure selection and performance assessment for disturbance rejection in MIMO processes," *Ind. Eng. Chem. Res.*, vol. 46, no. 26, pp. 9170–9178, Dec. 2007.

[5] J.-W. Chang and C.-C. Yu, "Relative disturbance gain array," *AIChE J.*, vol. 38, no. 4, pp. 521–534, Apr. 1992.

[6] H. Zhou, Y. Hao, and W. Tan, "Partially decentralized load frequency control of multi-area power systems in deregulated environments," in *Proc. 11th World Congr. Intell. Control Autom.*, Shenyang, China, Jun. 2014, pp. 4704–4709.

[7] M. E. Salgado and A. Conley, "MIMO interaction measure and controller structure selection," *Int. J. Control*, vol. 77, no. 4, pp. 367–383, Mar. 2004.

[8] F.-Y. Lin, J.-C. Jeng, and H.-P. Huang, "Multivariable control with generalized decoupling for disturbance rejection," *Ind. Eng. Chem. Res.*, vol. 48, no. 20, pp. 9175–9185, Sep. 2009.

[9] Q. B. Jin and Q. Liu, "Partial decoupling control for disturbance rejection for multivariable systems with time delays," *Ind. Eng. Chem. Res.*, vol. 53, no. 41, pp. 15932–15945, Oct. 2014.

[10] K. Ohishi, "Torque-speed regulation of DC motor based on load torque estimation," in *IEEJ Int. Power. Electron. Conf.*, Tokyo, Japan, 1983, pp. 1209–1216.

[11] K. Ohishi, M. Nakao, K. Ohnishi, and K. Miyachi, "Microprocessor-controlled DC motor for load-insensitive position servo system," *IEEE Trans. Ind. Electron.*, vol. IE-34, no. 1, pp. 44–49, Feb. 1987.

[12] B. Sarsembayev, K. Suleimenov, and T. D. Do, "High order disturbance observer based PI-PI control system with tracking anti-windup technique for improvement of transient performance of PMSM," *IEEE Access*, vol. 9, pp. 66323–66334, 2021.

[13] L. Sun, D. Li, and K. Y. Lee, "Enhanced decentralized PI control for fluidized bed combustor via advanced disturbance observer," *Control Eng. Pract.*, vol. 42, pp. 128–139, Sep. 2015.

[14] J. Yang, B. Wu, S. Li, and X. Yu, "Design and qualitative robustness analysis of an DOBC approach for DC-DC buck converters with unmatched circuit parameter perturbations," *IEEE Trans. Circuits Syst. I, Reg. Papers*, vol. 63, no. 4, pp. 551–560, Apr. 2016.

[15] K. Natori and K. Ohnishi, "A design method of communication disturbance observer for time-delay compensation, taking the dynamic property of network disturbance into account," *IEEE Trans. Ind. Electron.*, vol. 55, no. 5, pp. 2152–2168, May 2008.

[16] T. Umeno, T. Kaneko, and Y. Hori, "Robust servosystem design with two degrees of freedom and its application to novel motion control of robot manipulators," *IEEE Trans. Ind. Electron.*, vol. 40, no. 5, pp. 473–485, Oct. 1993.

[17] K. Hong and K. Nam, "A load torque compensation scheme under the speed measurement delay," *IEEE Trans. Ind. Electron.*, vol. 45, no. 2, pp. 283–290, Apr. 1998.

[18] Z. Hongdong, Z. Guanghui, and S. Huihe, "Control of the process with inverse response and dead-time based on disturbance observer," in *Proc. Amer. Control Conf.*, Portland, OR, USA, Jun. 2005, pp. 4826–4831.

[19] L. Wang and J. Cheng, "Robust disturbance rejection methodology for unstable non-minimum phase systems via disturbance observer," *ISA Trans.*, vol. 100, pp. 1–12, May 2020.

[20] N. H. Jo, H. Shim, and Y. I. Son, "Disturbance observer for non-minimum phase linear systems," *Int. J. Control, Autom. Syst.*, vol. 8, no. 5, pp. 994–1002, Oct. 2010.

[21] N. H. Jo, C. Jeon, and H. Shim, "Noise reduction disturbance observer for disturbance attenuation and noise suppression," *IEEE Trans. Ind. Electron.*, vol. 64, no. 2, pp. 1381–1391, Feb. 2017.

[22] E. Sariyildiz and K. Ohnishi, "A guide to design disturbance observer based motion control systems," in *Proc. Int. Power Electron. Conf. (IPEC-ECCE ASIA)*, Hiroshima, Japan, May 2014, pp. 2483–2488.

[23] E. Sariyildiz and K. Ohnishi, "Analysis the robustness of control systems based on disturbance observer," *Int. J. Control*, vol. 86, no. 10, pp. 1733–1743, May 2013.

[24] E. Sariyildiz and K. Ohnishi, "A guide to design disturbance observer based motion control systems," in *Proc. Int. Power Electron. Conf. (IPEC-Hiroshima-ECCE ASIA)*, Cape Town, South Africa, May 2014, pp. 5772–5777.

[25] Q. Liu, Q. Jin, B. Huang, and M. Liu, "Iteration tuning of disturbance observer-based control system satisfying robustness index for FOPTD processes," *IEEE Trans. Control Syst. Technol.*, vol. 25, no. 6, pp. 1738–1788, Nov. 2017.

[26] X. S. Chen, J. Yang, S. H. Li, and Q. Li, "Disturbance observer based multi-variable control of ball mill grinding circuits," *J. Process Control*, vol. 19, no. 7, pp. 1205–1213, Jul. 2009.

[27] P. Zhou, T. Y. Chai, and J. H. Zhao, "DOB design for nonminimum-phase delay systems and its application in multivariable MPC control," *IEEE Trans. Circuits Syst. II, Exp. Briefs*, vol. 59, no. 8, pp. 525–529, Aug. 2012.

[28] P. Zhou, W. Dai, and T.-Y. Chai, "Multivariable disturbance observer based advanced feedback control design and its application to a grinding circuit," *IEEE Trans. Control Syst. Technol.*, vol. 22, no. 4, pp. 1474–1485, Jul. 2014.

[29] W. Zhang, Y. Wang, Y. Liu, and W. Zhang, "Multivariable disturbance observer-based H_2 analytical decoupling control design for multivariable systems," *Int. J. Syst. Sci.*, vol. 47, no. 1, pp. 179–193, Jul. 2016.

[30] Q. Jin, W. Cai, and X. Du, "Improved disturbance observer-based control for multivariable processes with time delays based on modified inverse model," *Trans. Inst. Meas. Control*, vol. 42, no. 3, pp. 339–350, Feb. 2020.

[31] Q. Jin, W. Cai, and X. Du, "Disturbance observer-based control with partially coupled inverse model for stable TITO processes with time delays," *ISA Trans.*, vol. 110, pp. 148–159, Apr. 2021.

[32] M. Lee, K. Lee, C. Kim, and J. Lee, "Analytical design of multiloop PID controllers for desired closed-loop responses," *AIChE J.*, vol. 50, no. 7, pp. 1631–1635, Jul. 2004.

[33] V. V. Kumar, V. S. R. Rao, and M. Chidambaram, "Centralized PI controllers for interacting multivariable processes by synthesis method," *ISA Trans.*, vol. 51, no. 3, pp. 400–409, May 2012.

[34] T. N. L. Vu and M. Lee, "Independent design of multi-loop PI/PID controllers for interacting multivariable processes," *J. Process Control*, vol. 20, no. 8, pp. 922–933, Sep. 2010.

[35] B. A. Ogunnaike, J. P. Lemaire, M. Morari, and W. H. Ray, "Advanced multivariable control of a pilot-plant distillation column," *AIChE J.*, vol. 29, no. 4, pp. 632–640, Jul. 1983.

[36] Y. Shen, W.-J. Cai, and S. Li, "Multivariable process control: Decentralized, decoupling, or sparse?" *Ind. Eng. Chem. Res.*, vol. 49, no. 2, pp. 761–771, Jan. 2010.

[37] S. Ghosh and S. Pan, "Centralized PI controller design method for MIMO processes based on frequency response approximation," *ISA Trans.*, vol. 110, pp. 117–128, Apr. 2021.

WU CAI received the B.S. degree in automation and the Ph.D. degree in control science and engineering from the Beijing University of Chemical Technology, Beijing, China, in 2014 and 2021, respectively. Her research interests include coupling analysis, decoupling strategy, and disturbance rejection control theory of multivariable systems.

PENG SHEN received the Ph.D. degree in electrical power systems from the South China University of Technology, Guangzhou, China, in 2019. His research interests include power system stability analysis and control, and adaptive robust control and its application in power systems.

YUTING SHANG received the M.S. degree from the Guangdong University of Technology, Guangzhou, China, in 2006. He was engaged in intelligent equipment research and development with Zhuhai Gree Intelligent Equipment Company Ltd., from 2015 to 2021. His research interests include intelligent control system design, and robotics and applications.

XINGHAN DU received the B.S. degree in automation and the Ph.D. degree in control science and engineering from the Beijing University of Chemical Technology, Beijing, China, in 2013 and 2018, respectively. He joined Jiangsu Normal University, Xuzhou, China, in 2019, where he is currently a Lecturer with the College of Electrical Engineering and Automation. His current research interests include multivariable process control, disturbance observer-based control, and data-driven control.

• • •